Separation and Purification Technology 372 (2025) 133436

Contents lists available at ScienceDirect

Separation and Purification Technology

journal homepage: www.elsevier.com/locate/seppur

Nanostructured ceramic membranes for hydrogen separation☆

A. Bartoletti [a,b], E. Mercadelli [a,*], A. Gondolini [a], V. Saraceni [c,d], A. Fasolini [c,d], J. De Maron [c,d], F. Basile [c,e,**], A. Sanson [a]

[a] National Research Council of Italy, Institute of Science, Technology and Sustainability for Ceramics (CNR-ISSMC), Via Granarolo 64, 48018 Faenza, Italy
[b] Department of Chemical Sciences, Università degli Studi di Padova, Via Marzolo 1, 35131 Padova, Italy
[c] Department of Industrial Chemistry "Toso Montanari" University of Bologna, Viale Del Risorgimento 4, 40136 Bologna, Italy
[d] Center for Chemical Catalysis - C3, University of Bologna, Viale Del Risorgimento 4, 40136 Bologna, Italy
[e] Consorzio Interuniversitario per La Scienza e Tecnologia Dei Materiali (INSTM), Via G. Giusti, 9 50121 Firenze, Italy

ARTICLE INFO

Editor: Dr. B. Van der Bruggen

Keywords:
BCZY-GDC
Washcoating
Dip coating
Cer-cer composite membrane
H_2 permeation

ABSTRACT

Hydrogen separation membranes are cornerstone technologies for advancing the practical development of the hydrogen sector. Mixed ionic-electronic conductors (MIEC) based on $BaCe_xZr_yY_{1-x-y}O_{3-\gamma}$ (BCZY) perovskites and $Ce_zGd_{1-z}O_{2-\delta}$ (GDC) fluorite have gained increasing attention for their high conductivity and selectivity, temperature and chemical stability. However, hydrogen permeation fluxes reached until now are still too low for industrial applications (compared to metal-based or cer-met composites). One strategy to improve the separation performances is to enhance the catalytic activity by applying a nanostructured coating on the whole membrane surface, to increase the overall surface area of the membrane and provide for a better catalyst dispersion. This study aims to establish a reproducible and eco-friendly methodology for applying nanostructured BCZY-GDC porous coatings onto symmetric cer-cer membranes via dip-coating in aqueous suspensions, and investigate their influence on the hydrogen separation ability. It was found that hydrogen permeated flux increases by more than 2 times when a 3.5 μm porous coating was applied to both sides of the membranes, thanks to the better distribution of Pt catalytic particles. No signs of degradation or structural modification were observed on the porous coating after permeation.

1. Introduction

The "European Green Deal" presented by the European Commission in 2019 outlines the main policy initiatives to achieve net-zero global warming emissions by 2050 [1]. Hydrogen was identified as a key to achieving the Green Deal objectives, including the provision of clean, affordable and secure energy and the achievement of a carbon–neutral, clean and circular economy.

Despite the huge effort in the development of green technologies such as water electrolysers, about 99 % of hydrogen is produced worldwide from high-emission sources using fossil fuels [2]. Hydrogen produced in this way contains several impurities like CO, CO_2 and H_2S and needs additional steps of purification for process intensification and, more in general, for industrial and automotive applications where >99.999 % H_2 purity is required [3–5]. Depending on the efficiency of the H_2 purification step [6,7], this has a great impact on the H_2 generation price.

In this context, membrane technology represents an interesting answer for the rationalization of chemical productions thanks to its intrinsic characteristics of efficiency and operational simplicity, high selectivity, low energetic requirements, good stability under operating conditions and environmental compatibility, easy control and scale-up [8]. In particular, inorganic membranes can be integrated with many relevant industrial processes in two main areas: (i) gas separation to replace sorption-based processes in the purification of H_2; and (ii) membrane reactors coupling reaction and separation processes in one unit [9].

Mixed ionic-electronic conductor (MIEC) ceramic membranes based on $BaCe_{0.65}Zr_{0.20}Y_{0.15}O_{3-\delta}$ (BCZY) – $Ce_{0.8}Gd_{0.2}O_{2-\delta}$ (GDC) have gained increasing attention thanks to their pronounced stability in CO_2 [10] and H_2S [11] reach atmosphere, high mechanical strength [12,13], enhanced proton/electron conductivity, i.e. σ ((S cm^{-1}) x 10^{-3}) = 33.0

☆ This article is part of a special issue entitled: 'Inorganic Membranes' published in Separation and Purification Technology.

* Corresponding author.
** Corresponding author at: Department of Industrial Chemistry "Toso Montanari" University of Bologna, Viale Del Risorgimento 4, 40136 Bologna, Italy.
E-mail addresses: elisa.mercadelli@cnr.it (E. Mercadelli), f.basile@unibo.it (F. Basile).

https://doi.org/10.1016/j.seppur.2025.133436
Received 19 December 2024; Received in revised form 20 March 2025; Accepted 6 May 2025
Available online 7 May 2025

(in wet H_2), 122.6 (in dry H_2), 13.3 (in dry air) [14], and excellent hydrogen flux permeation [15]. The key characteristics of BCZY-GDC composite membranes are collected in Table 1 along with the main features of the conventional Pd-based membranes [16–18].

To avoid surface kinetics limitation (which is generally the rate-determining step) membranes are activated with metallic nanoparticles, typically platinum, to enhance the H_2 dissociation (at the feed) and the water splitting (at the sweep) reaction rates. Both mechanisms were found to contribute to the overall H_2 concentration at the permeate side and depend on the catalyst deposition method [19].

One strategy to improve the catalyst dispersion and enhance the overall surface area of the membrane is to deposit a catalytic porous layer on top of the membrane surface (also called "washcoat") [8]. The term "washcoat" is used to identify a nanostructured porous coating, generally applied to a ceramic support to provide a high surface area and facilitate the dispersion of catalytic metals [20]. The concept was developed to improve the performance of monolithic catalysts such as foams or honeycomb-type supports, in processes including the purification of automobile exhaust gas, elimination of volatile organic compounds and the catalytic combustion of methane [21–23].

Regarding the field of gas separation membranes or catalytic membrane reactors, the use of the washcoating was widely investigated for oxygen permeable membranes [24,25], while Escolastico et al. [26] investigated for the first time the effect of catalytic porous layers in proton conductive ceramic membrane reactors based on $La_{5.5}WO_{11.25-\delta}$/$La_{0.87}Sr_{0.13}CrO_{3-\delta}$. The application of a 20 μm $La_{0.75}Sr_{0.15}Ce_{0.1}CrO_{3-\delta}$ screen printed layer on the top of the dense membrane infiltrated with Ni nanoparticles, was found to boost by a factor of 10 the hydrogen permeation flux at 700 °C of the bare membrane.

This work aimed to understand the impact of a nanostructured porous coating deposited on both sides of symmetric BCZY-GDC membranes on hydrogen separation efficiency. Here, a protocol for manufacturing stable BCZY-GDC aqueous suspensions and their subsequent deposition by dip coating was developed for the first time. Despite being a batch process, dip coating permits the obtaining of nanostructured layers with variable thicknesses from 0.1 to 50 μm [27,28] depending on the characteristics of the suspension and the operating conditions, and is not limited to planar and dense substrates like screen printing. The optimization of the whole process led to the production of symmetric membranes covered by a defect-free, porous, nanostructured layer with micrometric thickness, showing enhanced hydrogen permeability if compared to the bare BCZY-GDC membrane.

Table 1
Key characteristics of BCZY-GDC membranes, with select data taken from [16–18] on Pd-based membranes included for comparison.

	BCZY-GDC membranes	Pd-based membranes
H_2 selectivity	>1000	>1000
H_2 flux*	6–80	60–300
Transport mechanism	Solution/diffusion (Proton and electron conduction)	Solution/Diffusion
Operational temperature	550–1000 °C	300–600 °C
Stability in CO_2	Stable H_2 flux at 750 °C, for 100 h, using wet 15 vol% CO_2 in Ar as sweep gas; 100 % full recovery after removal	From 70 to 100 % recovery after CO_2 removal
Stability in H_2S	conductivity drop of 2 % at 700 °C, under 700 ppm of H_2S	Poisoning: decrease of 1 order of magnitude at 400–450 °C with 20–100 ppm, 1–24 h of testing
Mechanical strength	Flexural strength of ≈ 70 MPa @750 °C. Nano-hardness of 12.8 ± 2.1 GPa for GDC and 9.2 ± 1.9 GPa for BCZY.	Dependent on the nature of porous support. For thin foils: tensile strength σ (MPa) of 890–1590 at 25–450 °C; nanoHardness ≈ 3 GPa

* 10^{-3} mol m^{-2} s^{-1} at pressure diff. = 1 bar.

2. Experimental

2.1. Materials

Symmetric membranes were produced using $BaCe_{0.65}Zr_{0.20}Y_{0.15}O_{3-\delta}$ (BCZY, s.s.a. = 4.92 m^2 g^{-1} and d_{50} = 1.1 μm, Marion Technologies) and $Ce_{0.8}Gd_{0.2}O_{2-\delta}$ (GDC, s.s.a. = 5.60 m^2 g^{-1} and d_{50} = 0.21 μm Fuel Cell Materials) as starting ceramic powders, and ZnO nanopowders (Sigma Aldrich) as sintering aid. For the production of the nanostructured coating (i.e. washcoating), BCZY (s.s.a. = 13.40 m^2 g^{-1} and d_{50} = 0.73 μm, Marion Technologies) and GDC (s.s.a. = 35.60 m^2 g^{-1} and d_{50} = 1.09 μm, Fuelcellmaterials) were considered as the starting ceramic powders, Darwan 821A (RT Vanderbit), Polyvinyl alcohol (PVA, MW = 85,000–124000, Sigma Aldrich), and Surfynol SE-F (Evonik Industries) as the deflocculant, binder, and surfactant respectively. Anhydrous ethanol (99.99 %, Sigma Aldrich) was used for mixing the starting ceramic powders, while isopropanol (Sigma Aldrich) was considered for the measurement of the density through the Archimedes method.

2.2. Membrane manufacturing

Symmetric membranes were produced by dry pressing. First, BCZY and GDC in 1/1 vol% ratio were previously ball milled in ethanol with 1 wt% ZnO as a sintering aid. The resulting powder was dried, sieved at 200 μm, and uniaxially pressed in a Ø = 20.0 mm die at 750 Kg cm^{-2}, and isostatically pressed at 3000 bar at room temperature [29]. The green pellets were finally sintered at 1550 °C for 4 h in a BCZY-GDC-rich atmosphere, i.e., placing the samples on a BCZY-GDC powder bed and covering them with the same sacrificial powder as already reported in [29]. The relative density measured by Archimedes' method in isopropanol was 97 ± 1 %. The final membranes' thickness (in the 600–650 μm range) was achieved by mechanical polishing using a semi-automatic lapping machine Tegramin (Struers) equipped with 500 and 1200 SiC grinding discs. Membranes used for contact angle measurements were also polished using progressively finer abrasive diamond suspensions up to 1 μm.

2.3. Optimization of the slurry for the washcoating process

A BCZY-GDC slurry was developed for deposition onto both faces of the membrane, producing a nanostructured BCZY-GDC coating (i.e., washcoat).

Different water-based slurries were produced by sonication (Sonicator, ultrasonic processor XL) as shown in **Fig. S1**. The amount of deflocculant and binder was firstly optimized throughout viscosity analyses [30], fixing the solid loading at 5 wt%; the surfactant amount was evaluated through contact angle measurements. PVA was used as a 30 wt% water-based solution obtained by mixing PVA powders in water under vigorous stirring at 80 °C for 3 h. BCZY and GDC were previously mixed by ball-milling in ethanol and sieved at 75 μm before the preparation of the slurries.

2.4. Deposition of the nanostructured coating

BCZY-GDC washcoats were obtained by immersing membranes for 3 min in the slurry through a home-made dip coater (**Fig. S2 a**) at different withdrawal speeds (1 – 7 mm s^{-1}), followed by centrifugation using a spin coater apparatus (POLOS Spin 150i-NPP, SPS Europe) to remove the excess of solution and baked at 110 °C. Before depositions, samples were wrapped in a copper wire (**Fig. S2 b**) and fixed to the sample holder with a clip. The process was repeated until the desired thickness (1–5 μm range) was reached, and the coatings were then finally consolidated at 900 °C (50 °C h^{-1}) for 4 h in air.

2.5. Characterizations

Rheological measurements were performed to optimize the amount of deflocculant and binder by using a controlled-stress rotational rheometer (Bohlin C-VOR 120, Bohlin, Malvern Instruments) equipped with a concentric cylinder according to DIN 53019/ISO 3219 in a controlled stress mode from 0.01–100 Pa, at 25 °C.

The isoelectric point of the washcoat suspension was determined through Dynamic Light Scattering (DLS) and Electrophoretic Light Scattering (ELS) using a Zetasizer Nanoseries (Malvern Instruments) at 25 °C, which can simultaneously determine the nanoparticles' size and their zeta potential. During the analysis, the pH was automatically adjusted using diluted solutions of NaOH (Merck) and HCl (Merck), at 1 M and 0.01 M concentrations.

Contact angle measurements were conducted to optimize the surfactant content, by using a Drop Shape Analyser (DSA30 Tensiometer, Krüss) in pendant drop configuration system, by dropping the produced suspensions on planar and polished BCZY-GDC dense pellets.

After thermal treatments, washcoats were characterized by XRD analysis (D8 ADVANCE, LynkEye Detector-Bruker AXS, Germany) using CuKα radiation in the 20–80° 2θ range and a scan rate of 0.02°.

The microstructure of the nanostructured coatings was analysed by a scanning electron microscope ΣIGMA SEM-FEG (Zeiss) equipped with INCA ENERGY 350 microdetector (EDX) and INCASmartMap system. SEM-EDX analysis was conducted also on the membranes after permeation tests. ImageJ software was used to calculate both the mean particle size and the thickness of the deposited coating after thermal treatment.

2.6. Hydrogen permeation tests

Permeation measurements were performed on disk-shaped samples to assess hydrogen permeation over a temperature range between 400 and 750 °C as previously reported [19]. The testing setup consisted of a double-chamber quartz reactor, with separate feed and sweep sections. Silver alloy rings (10 % Cu and 90 % Ag) were used for sealing. The sealing ring is produced in the laboratory by shaping and welding a 1 mm commercial wire to match the reactor's required diameter. The sealing is achieved through a controlled heating process: a ramp-up at 120 °C h^{-1} to 750 °C, followed by an overnight hold at 750 °C, a one-hour soak at 765 °C, and then cooling back to 750 °C.

A gas mixture of H_2 and He was used for the feed, while Ar served as the sweep gas. The flow rates for the feed and sweep gases were controlled by mass flow controllers (MFC) at 80 mL min^{-1} and 150 mL min^{-1}, respectively, with both gases humidified to saturation at 28 °C. A basic schematic of the permeation system is shown in Fig. 1.

The hydrogen concentration at the permeate side was measured at the reactor outlet using an Agilent Technologies 490 Micro GC with a Molsieve5A capillary module. The results presented were obtained at steady state after 30 min of stabilization while the temperature was monitored using a thermocouple placed near the membrane. The quality of the sealing was assessed by monitoring the He content in the permeate, and the results were considered acceptable if the He leakage was below 5 %. Hydrogen leaks were subtracted from the permeation data. The hydrogen permeability of the membranes was characterized by different hydrogen partial pressures at high temperatures with humidified fluxes. Typically, the hydrogen flux through a mixed proton–electron conducting membrane is represented by the Wagner equation (1):

$$J_{H2} \approx \frac{RT}{4F^2L}\frac{(\sigma_{H^+}+\sigma_{O^{2-}})(\sigma_e+\sigma_h)}{\sigma_T}\ln\frac{p(H_2 feed)}{p(H_2 sweep)} \quad (1)$$

Due to surface kinetic effects that limit permeation, the membranes were activated with Pt, as a typical catalyst for these kinds of membranes [10,14,19,31] to enhance both hydrogen dissociation and water splitting reactions. Specifically, both sides of bare membranes (i.e., dense BCZY-GDC pellets without washcoating) and washcoated membranes (dense pellets functionalized with a BCZY-GDC coating deposited by dip coating) were activated via drop-casting impregnation using an aqueous solution containing 4.23 × 10^{-3} mol L^{-1} of Tetraammineplatinum(II) nitrate (Premion®, 99.99 %). The membranes were then dried in an oven at 50 °C for 1 h, yielding a Pt deposition of 0.15 mg cm^{-2}, as detailed elsewhere [19]. The deposited precursor was subsequently reduced to metallic Pt directly in the reactor during the sealing procedure under a 50 % H_2/He atmosphere, with a ramp rate of 120 °C h^{-1} up to 750 °C. Additionally, washcoated membranes without Pt were tested for comparison.

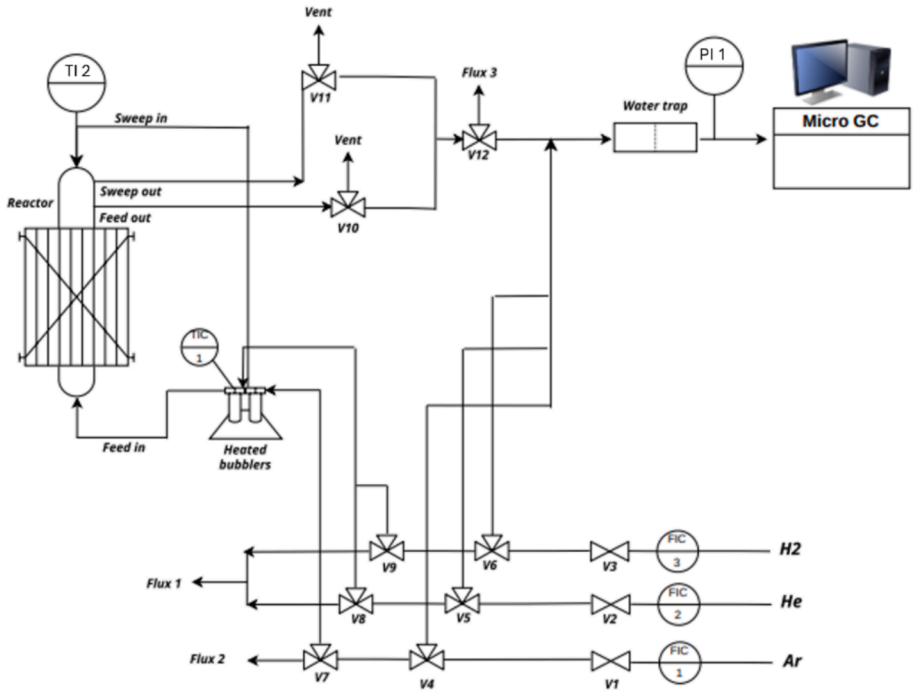

Fig. 1. Schematic representation of permeation tests set up.

3. Results and discussions

3.1. Slurry optimization

The type of additives was selected based on the previous works [32–34], while the amount of binder and dispersing agent was assessed by viscosity analyses. On the other hand, the quantity of surfactant was evaluated through contact angle measurements. The optimization study of the BCZY-GDC slurry formulation was firstly conducted using suspensions with the 5 wt% of ceramic content. Darwan 821-A was selected as effective dispersant for the BCZY-GDC system based on previous experience [34].

In Fig. 2**a**, the viscosity curves of the BCZY-GDC suspensions with different amounts of dispersant are reported. The suspension without dispersant exhibits shear-thinning behaviour up to 400 s^{-1} likely due to particle deagglomeration as the shear rate increases. At higher shear rates, viscosity begins to increase due to turbulence generated within the conical cylinder, making it difficult for the rotational rheometer to accurately measure viscosity at these conditions [35]. Similar results were obtained when a small amount of 0.1 10^{-3} $g_{dispersant}$ m^{-2}_{powder} was added. This provides for a slight decrease in the viscosity of the suspension which still presents a non-Newtonian behaviour.

For the curves recorded with suspensions containing 0.5 to 10 × 10^{-3} $g_{dispersant}$ m^{-2}_{powder} a strong stabilization effect is observed, and the viscosity curves show the same trend: an initial decrease in viscosity down to ≈ 10 s^{-1} followed by stable values up to 30 s^{-1}. At this shear rate, instrumental artifacts were observed as previously discussed, which occur at lower shear rates due to the reduced viscosity. The initial decrease in viscosity is attributed to two factors: the well-known inertia of the controlled-stress rheometer at very low shear rates [36,37], which tends to be more pronounced when using concentric conical cylinders [38], and the low torque (~10^{-6} N·m) generated by suspensions containing ≥ 0.5 × 10^{-3} $g_{dispersant}$ m^{-2}_{powder}, which is close to the rheometer's instrumental limit (~10^{-7} N·m).

To provide the best compromise between the lower slurry viscosity and amount of dispersant, curves were compared at 30 s^{-1}. This value was selected since it falls inside the typical range of shear rate of the dip coating process, and it is the highest shear rate value of the plateaux of the curves containing ≥ 0.5 × 10^{-3} $g_{dispersant}$ m^{-2}_{powder}. Particularly, the best compromise between stabilization at 30 s^{-1} and dispersant concentration is obtained at 1 × 10^{-3} $g_{dispersant}$ m^{-2}_{powder} as reported in Fig. 2**b**. Moreover, optimal viscosity values for the dip coating process [35,39] were reached by increasing the amount of PVA up to 5 wt% (Fig. 2**c**). The increase in PVA concentration gradually extends the range

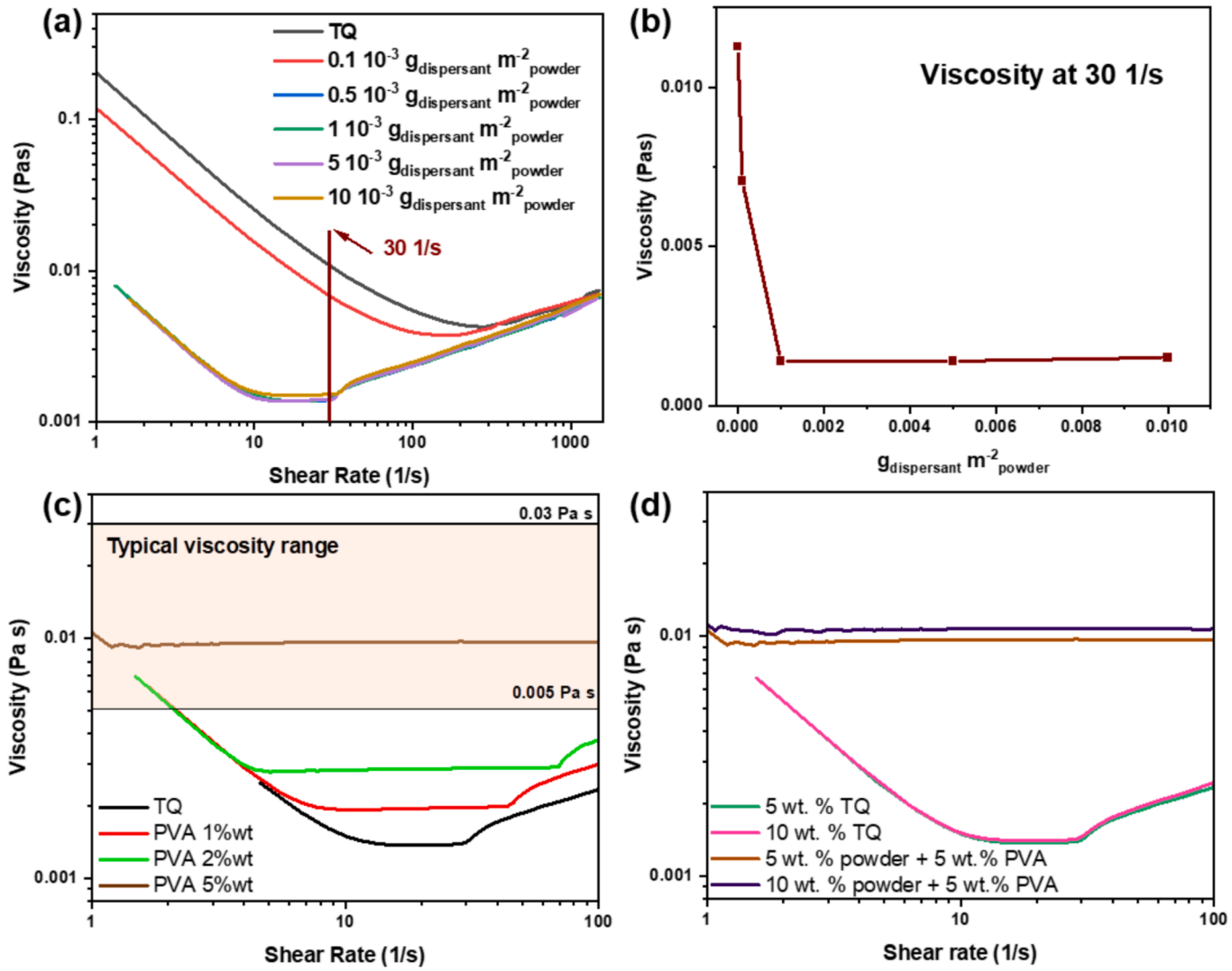

Fig. 2. Viscosity/shear stress curves of the BCZY-GDC suspensions with 5 wt% solid content with different amounts of dispersing agent (a) and viscosity of the obtained suspensions at 30 s^{-1} (b); flow curves at different PVA concentrations (c) and comparison with the slurry having the 10 wt% solid content (d). Suspensions prepared without additives are denoted as TQ.

of measure of the suspension (i.e. the observable Newtonian behaviour) as an increase in viscosity mitigates both the inertia of the system [36] and instrumental artifacts at high shear rate values.

An increase in the solid content of the suspension at 10 wt% (Fig. 2**d**) did not affect the viscosity behaviour of the slurries. The addition of the same PVA concentration (5 wt%) to the 10 wt% powder suspension leads to viscosity values and behaviour very similar to that of the 5 wt% powder suspension and suitable for the dip-coating process. For this motivation, both 5 and 10 wt% (with 5 wt% of PVA) powder suspensions were considered for the further tests.

The amount of surfactant was evaluated for preventing the formation of bubbles, detrimental to the production of a homogenous coating. In our previous work [19], we found out that BCZY-GDC-based ceramics show a greater affinity towards nonpolar substances, therefore the wettability of the membranes with polar liquids like water is expected to be low. To tackle this problem, several slurries with different amounts of Surfynol SE-F were produced and dropped onto dense polished membrane surfaces for contact angle measurements. As shown in Fig. 3 **a**, the increasing of the amount of surfactant (from 0 to 0.15 wt%) leads to an enhanced wettability and time-stability of the drops produced. An optimal concentration of 0.15 wt% was selected, effectively eliminating bubbles in the slurry caused by the PVA solution.

The abovementioned optimization process leads to the formulation of two slurries with different solid contents (5 and 10 wt%) as reported in Table 2.

The optimized slurry was finally characterized by DLS-ELS (Fig. 3**b, c**). The suspension was found to be slightly alkaline with a pH = 8.1 and

Table 2
Slurry composition expressed in wt. % for the preparation of the washcoat.

Components	Role	Slurry W1 (5 wt%)	Slurry W2 (10 wt%)
BCZY-GDC	Ceramic powder	5.01	10.03
Water	Solvent	89.58	84.56
Darvan 821A	Deflocculant	0.15	0.15
Surfynol SE-F	Surfactant	0.15	0.15
PVA	Binder	5.11	5.11

ζ = -21,6 ± 0,5 mV, which is considered high enough to not incur particle flocculation/agglomeration during time as the isoelectric point was detected at pH ≈ 4 (Fig. 3**b**). No sign of suspension instability was observed also after one week of storage at RT. The suspension presents a monomodal distribution of particles centered at the submicrometric size of 137 ± 63 nm (Fig. 3**c**) suitable to produce nanostructured coatings.

3.2. Production of nanostructured washcoatings

The processing parameters were optimized using dense membranes fabricated by dry pressing. Before depositions, samples were polished using 1200 SiC foils to standardize the surface roughness of the substrates.

The consolidation temperature of the washcoat was set at 900 °C to completely decompose the $BaCO_3$ impurities present in the as-receive commercial BCZY powder, as shown in the XRD pattern of **Fig. S3**.

Different extraction speeds (v_0), such as 1, 3, 5, and 7 mm s^{-1} were

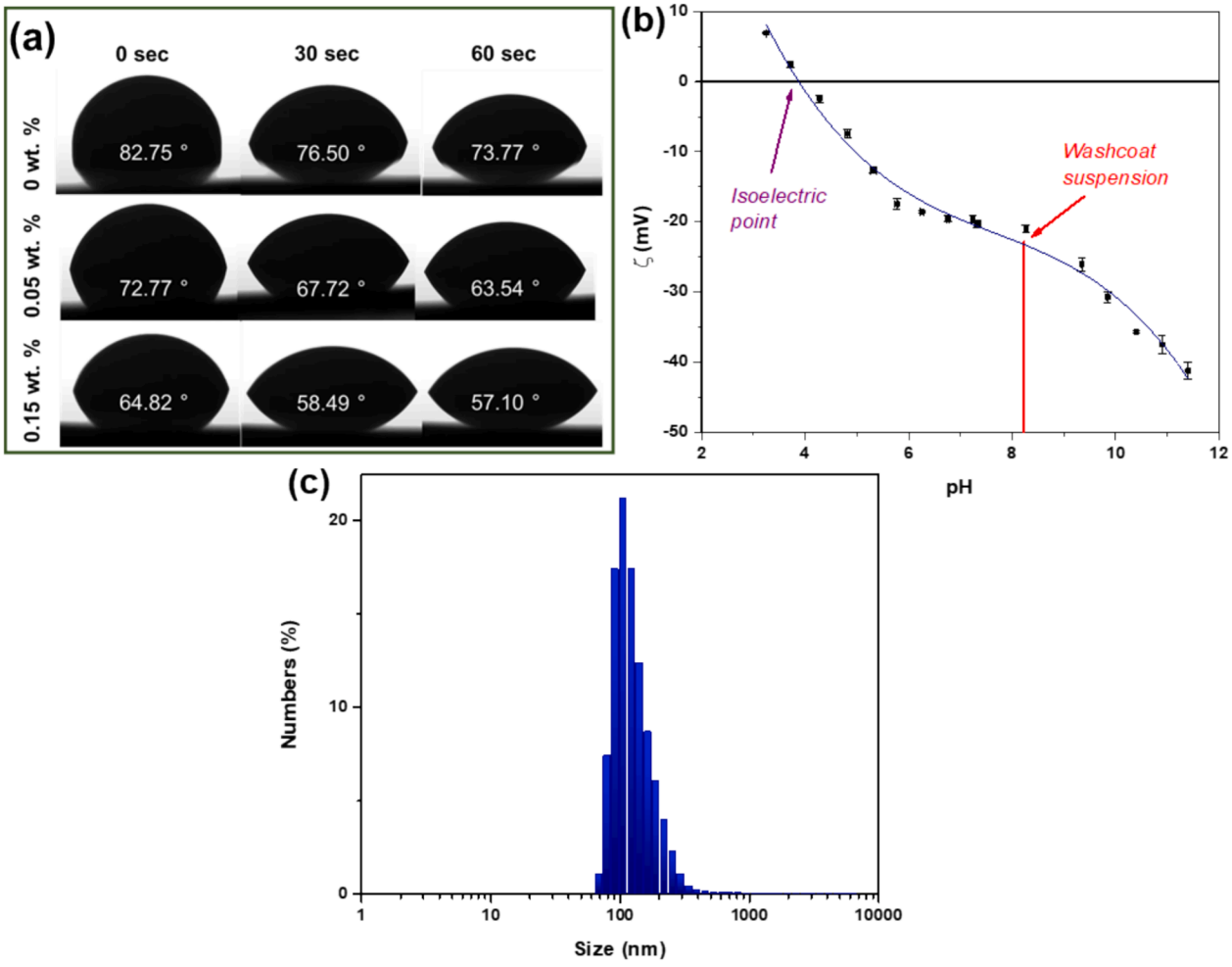

Fig. 3. Contact angles of different suspensions with increasing amounts of surfactant onto BCZY-GDC pellets (a); DLS-ELS analysis of the optimized suspension: Zeta potential vs pH (b) and hydrodynamic particle size distribution (c).

applied in order to obtain homogeneous porous coatings with micrometric thickness. In these conditions (Newtonian fluid and $v_0 > 1$ mm s^{-1}) the thickness of the layer obtained is mainly controlled by the withdrawal speed [40]. Fig. 4 compares the resulting coatings of the sample surface after three depositions at different v_0 values using Slurry W1 (5 wt% solid content suspension) with the bare surface.

The results suggest that the use of a diluted ceramic suspension, leads to an incomplete coating of the pellet surface regardless the different withdrawal speeds, leaving visible holes and streaks caused by the grinding process. However, as expected, an increase in the withdrawal speed led to the deposition of more active material, as shown in the SEM micrographs. Films with higher solid loading were observed for $v_0 =$ 5–7 mm s^{-1}, although a full coverage is not achieved even at these conditions.

To address this issue, the suspension with a higher solid content (Slurry W2, 10 wt% solid content suspension) was used for dip coating. Fig. 5**a–d** shows the SEM micrographs at different magnifications of the washcoat obtained after three dips at 7 mm s^{-1} using the Slurry W2 (10 wt% solid content suspension). With these conditions, the whole surface of the membranes is fully covered by the porous nanostructured washcoat. The mean particle size of the washcoat, calculated through image analysis, was 37 ± 18 nm. This datum is comparable with the particle size of the starting raw powders (**Fig. S4**) used to prepare the aqueous suspensions, confirming that no coarsening effects occur during the thermal treatment, preserving the nanometric structure of the final washcoat.

The thickness of the obtained coatings was calculated through image analysis of the corresponding SEM micrographs and found to be ≈1.75

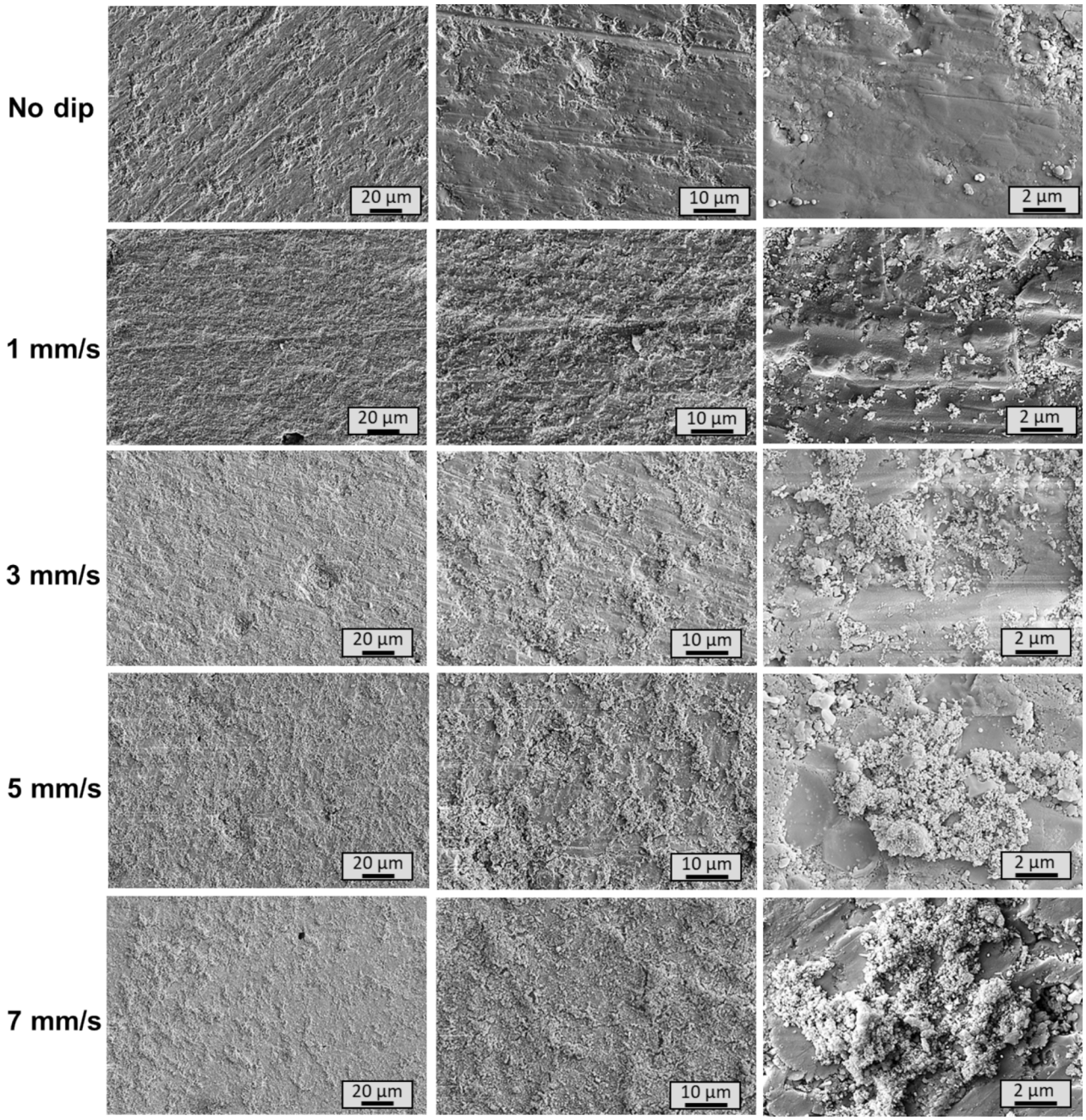

Fig. 4. SEM micrographs of the washcoat obtained after three deposition cycles with the 5 wt% suspension (Slurry W1) at different withdrawal speeds after thermal treatment at 900 °C; for each velocity different magnifications are shown.

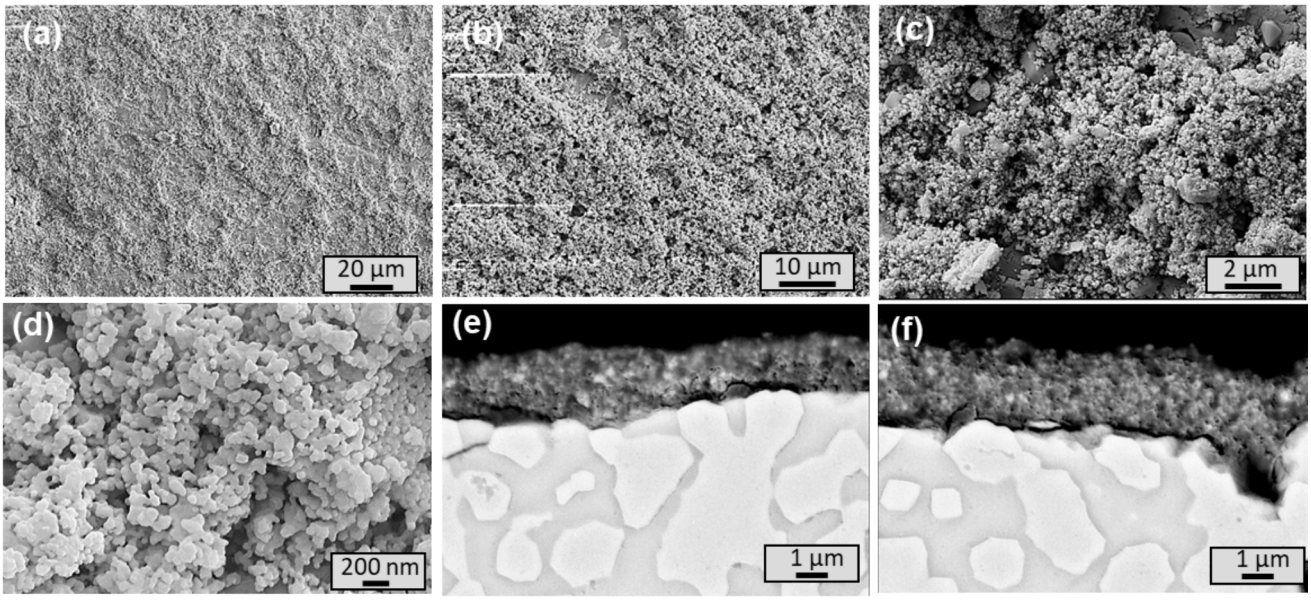

Fig. 5. SEM micrographs at different magnifications of the washcoat obtained after 3 dips into the 10 wt% suspension at the maximum v_0 (a-d); vertical polished cross sections of the as-produced coating using slurry W1 (e) and W2 (f) at 7 mm s^{-1}.

µm (Fig. 5**e)** and ≈3.5 µm (Fig. 5**f)** after three depositions at 7 mm s^{-1} with the suspension containing 5 wt% and 10 wt% solid loading, respectively. The SEM-BSE analysis of the cross sections (Fig. 5**e and f**) also evidences a homogeneous distribution, in the BCZY-GDC substrate (pellet), of light grey areas related to the GDC phase as well as dark areas attributed to BCZY. The peculiar topography of the polished cross-sections of the BCZY-GDC pellet is the result of the hardness contrast between the harder GDC (light grey) and the softer BCZY (dark) as already observed in [10,15].

Finally, it's worth mentioning that removing the excess of solution after each dip coating step was found to be mandatory to obtain homogeneous layers after thermal treatments (**Fig. S5**).

3.3. H_2 permeation tests

The effect of the porous coating on a BCZY-GDC dense membrane on the hydrogen permeation was investigated, comparing the performances of a symmetric dense pellet with (BCZY-GDC-WC) and without (BCZY-GDC, i.e. bare membrane) the washcoating. The two samples were activated with 0.15 mg cm^{-2} of Pt on both sides following a previously optimized methodology [19,32] briefly reported in the experimental section, and their hydrogen permeability was evaluated at different hydrogen feed concentrations and temperatures.

Results are reported in Fig. 6 where each graph shows data obtained with a selected composition of feed gas (50 % and 80 % of H_2 in He, vol. %) and correlates permeation values with temperature. As expected, the hydrogen flux rises at higher temperatures and by increasing the hydrogen concentration in the feed stream, following the Wagner equation (1). Previous studies [14–16] highlighted how two main phenomena contribute to hydrogen production on the sweep side: (i) hydrogen dissociation into proton and electrons on the membrane surface and their permeation through the membrane; and (ii) water

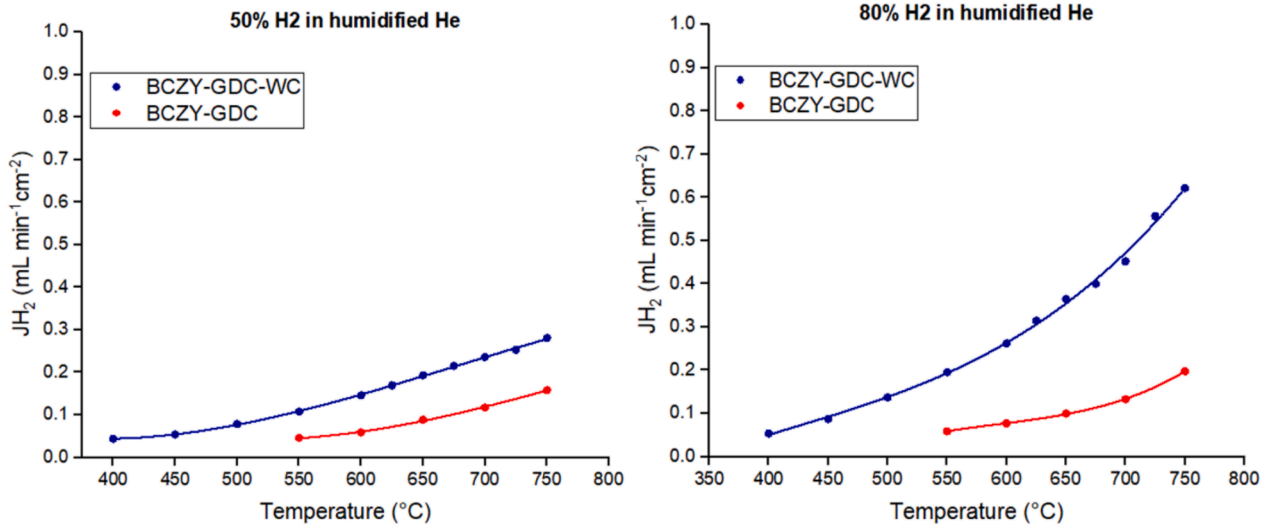

Fig. 6. H_2 flux (mL min^{-1} cm^{-2}) as a function of temperature and feed composition (50 % and 80 % of H_2 in He, %vol) for BCZY-GDC dense membrane (thickness = 640 ± 30 µm) and BCZY-GDC-WC washcoated dense membrane (thickness = 610 ± 30 µm), both activated with Pt. All the currents are humidified to saturation at 28 °C.

splitting (WS) reactions catalyzed by the presence of Pt particles. These contributions are known to be temperature-dependent, both favoured at high temperatures. Specifically, WS reaction becomes the most significant phenomenon at temperatures above 600 °C, while proton transport dominates over WS at temperatures below 600 °C. The BCZY-GDC symmetric dense membrane does not show a pronounced WS effect at temperatures above 600 °C, whereas the BCZY-GDC-WC membrane exhibits a much more noticeable WS effect. This is attributed to the presence of a micrometric porous layer on both sides of the membrane which limits mass transfer phenomena and promotes the reaction. In addition, the BCZY-GDC-WC membrane also displays improved performance at lower temperatures, which is crucial for practical applications.

The significant increase observed in the membrane with the washcoating can be attributed to several key phenomena. As previously mentioned, at elevated temperatures, water splitting becomes the dominant process. The species generated by water dissociation at the permeate side surface are H^+, O^{2-}, and e^-. An increase in the H_2 concentration in the retentate to 80 % boosts the flux of H^+ ions that permeate the surface, raising the concentration of H^+ on the permeate surface. This elevated H^+ concentration facilitates the recombination of H^+ ions from both water dissociation and hydrogen permeation, favouring their recombination over the formation of water with O^{2-} ions. Simultaneously, the O^{2-} species generated by water dissociation at the permeate surface are consumed in greater quantities at the retentate surface due to the increased H_2 concentration. This enhances the permeation of O^{2-} toward the retentate side, further promoting water splitting at the permeate side. These processes are less pronounced in the case of the pellet, as water splitting does not occur efficiently in the absence of a porous layer.

On the other hand, the porous and nanostructured nature of the washcoating enhances the available surface area for hydrogen dissociation and WS, even in the absence of Pt, demonstrating the washcoating technique as an effective tool for improving hydrogen permeation. This is evident from the comparison of a washcoated membrane tested without Pt activation (Fig. 7), which outperforms the platinum-activated bare membrane. However, the addition of Pt to washcoated membranes creates a synergistic effect, yielding the highest performance. In fact, the washcoating not only improves Pt dispersion but also increases the membrane's active surface area. BET analyses revealed an increase in specific surface area from less than 0.5 $m^2\ g^{-1}$ for the bare membrane to 6 $m^2\ g^{-1}$ for the washcoated membrane.

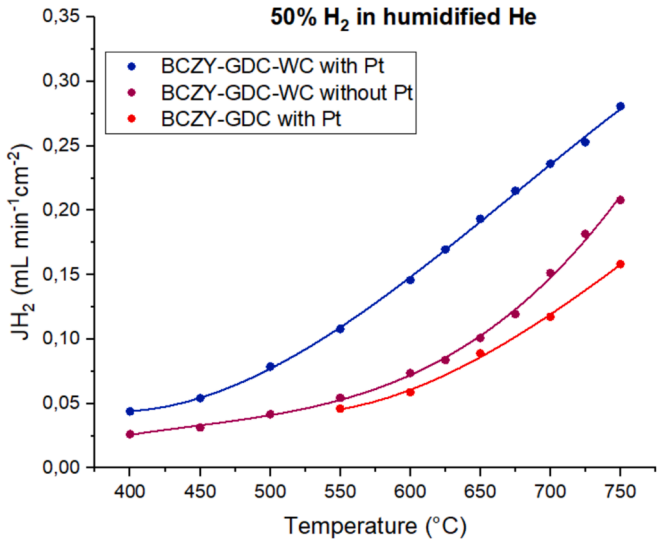

Fig. 7. H_2 flux (mL min^{-1} cm^{-2}) as a function of temperature with feed composition 50 % H_2 in He, %vol for BCZY-GDC dense membrane with Pt, BCZY-GDC-WC washcoated dense membrane with Pt and BCZY-GDC-WC washcoated dense membrane without Pt. Both currents are humidified to saturation at 28 °C.

Table 3 collects literature data on state-of-the-art all-ceramic membranes with a symmetric architecture (dense pellets). Hydrogen permeability in ceramic membranes is influenced by several interrelated factors. First, membrane thickness is a crucial parameter; as thickness increases, permeability generally decreases, leading to higher resistance to flow. The composition of the feed gas also plays a significant role in permeability; a higher hydrogen concentration in the feed raises the partial pressure on the membrane surface, thereby improving flux. However, the membrane's ability to dissociate and transport hydrogen is also dependent on the catalyst used. Furthermore, the sweep gas, which removes permeated hydrogen from the opposite side of the membrane, helps maintain a high concentration gradient, facilitating hydrogen transport. Additionally, the presence of water vapor (pH_2O) can enhance hydrogen availability at the permeate side if the water splitting reaction occurs. These variables contribute to the diverse results reported in the literature, as summarized in the Table 3, which highlights the effects of these parameters. In general, comparing results from different laboratories is challenging due to variations in experimental setups and conditions, as well as limited details on experimental parameters, especially the exact amount of platinum deposited on the membranes. Since the amount of platinum deposited has been shown to significantly impact performance [19], it is strongly recommended to always report the platinum deposition amount and method, and to establish standardized conditions for more reliable comparisons.

Nevertheless, to facilitate comparison, the normalized hydrogen flux (J^*_{H2}) was calculated from the reported J_{H2} in each cited article. Specifically, J_{H2} was multiplied by the sample thickness (d) to obtain J·d (J^*_{H2}), representing the amount of hydrogen (mL) permeated per unit area (cm^2), unit thickness (cm), and unit time (min). This normalization ensures a reliable comparison across membranes with varying thicknesses. It's worth mentioning that the H_2 separation flux reported here for the BCZY-GDC-WC membrane is among the highest reported in the literature concerning dense ceramic membranes. The superior hydrogen separation capability of the BCZY-GDC-WC membrane can be ascribed to the better dispersion of the Pt active phase (Fig. 8) thanks to the presence of the microporous layer which plays a key role in facilitating the dispersion of the Pt particles, increasing the available surface area, improving the interaction with the solvent during the impregnation process, and limiting the coarsening of the nanocatalyst (Fig. 8**d**). This results in a more homogeneous distribution of the precursor on the membrane, favouring its permeation performances and highlighting the improvement given by an optimized washcoating on the membrane surfaces.

Post-mortem SEM-FEG analysis coupled with EDX microanalysis (**Fig. S6**) was conducted to evidence eventual modifications of the coating layer. The washcoating remains with a nanometric size, and the platinum is found to be well distributed confirming that no structural modifications occurred during the permeation tests. Additionally, no peeling, damage, nor removal/detachments occur after the permeation tests.

The activation energies (Ea) for H_2 transport and water splitting were calculated (Table 4) using the Arrhenius equation (2), while the Arrhenius plots are reported in Fig. 9.

$$J_{H_2} = J_0 \exp\left(\frac{-Ea}{RT}\right) \quad (2)$$

At lower temperatures, the dominant mechanism is proton and electron transport, while at higher temperatures (above 650 °C), the water splitting process also occurs. Therefore, the activation energy was calculated separately for temperatures above and below this threshold [15,19,32].

Comparing the two membranes, activated with Pt, tested in this study, higher activation energy values (both high and low temperatures) were obtained for the bare BCZY-GDC compared to the washcoated

Table 3
Summary of performances of different hydrogen separation symmetric membranes produced by dry pressing. The normalized J^*_{H2} was calculated from the reported J_{H2} at 700 °C in each cited article.

System	Thickness [mm]	J_{H2} [ml cm^{-2} min^{-1}]	J^*_{H2} [ml cm^{-1} min^{-1}]	Catalyst	Feed gas [ml min^{-1}]	Sweep gas [ml min^{-1}]	pH_2O	*Ref.*
$BaCe_{0.8}Y_{0.2}O_{3-\delta}$ −$Ce_{0.8}Y_{0.2}O_{2-\delta}$	1.44	≈ 0.001	1.44 10^{-4}	No catalyst	100 (50 % H_2 in He)	100 (Ar)	0.03	[41]
$BaCe_{0.65}Zr_{0.2}Y_{0.15}O_{3-\delta}$ −$Ce_{0.85}Gd_{0.15}O_{2-\delta}$	0.65	0.15	9.75 10^{-3}	20 μm Pt layer screen printed on both side	100 (50 % H_2 in He)	150 (Ar)	0.03	[14]
$BaZr_{0.1}Ce_{0.7}Y_{0.1}Sn_{0.1}O_{3-\delta}$-$Ce_{0.9}Gd_{0.1}O_{2-\delta}$	0.65	0.03	1.95 10^{-3}	Pt layer screen printed on both side	100 (50 % H_2 in He)	100 (Ar)	dry	[42]
$50La_{5.5}WO_{11.25-\delta}$ − $50La_{0.87}Sr_{0.13}CrO_{3-\delta}$	0.37	0.15	5.55 10^{-3}	Pt layer screen printed on both side	100 (50 % H_2 in He)	150 (Ar)	0.025	[31]
$60La_{5.5}WO_{11.25-\delta}$ − $40La_{0.87}Sr_{0.13}CrO_{3-\delta}$	0.36	0.17	6.12 10^{-3}	Pt layer screen printed on both side	100 (50 % H_2 in He)	150 (Ar)	0.030	[26]
$La_{5.5}W_{0.8}Re_{0.2}O_{11.25-\delta}$	0.76	0.07	5.32 10^{-3}	20 μm Pt layer screen printed on both side	n.r. (50 % H_2 in He)	n.r. (Ar)	0.025	[43]
$BaCe_{0.8}Eu_{0.2}O_{3-\delta}$-$Ce_{0.8}Y_{0.2}O_{2-\delta}$	0.50	0.40	2.00 10^{-2}	Pt layer screen printed on both side	n.r. (50 % H_2 in He)	n.r. (Ar)	0.042	[44]
$BaCe_{0.65}Zr_{0.2}Y_{0.15}O_{3-\delta}$ −$Ce_{0.80}Gd_{0.20}O_{2-\delta}$ (BCZY-GDC)	0.64	0.12	7.68 10^{-3}	Impregnation of 0.15 mg/cm^2 Pt aqueous solution on both side	80 (50 % H_2 in He)	150 (Ar)	0.037	This work
$BaCe_{0.65}Zr_{0.2}Y_{0.15}O_{3-\delta}$ −$Ce_{0.80}Gd_{0.20}O_{2-\delta}$ (BCZY-GDC-WC)	0.61	0.24	1.46 10^{-2}	3.5 μm thick, porous washcoating, impregnation of 0.15 mg/cm^2 Pt aqueous solution on both side	80 (50 % H_2 in He)	150 (Ar)	0.037	This work

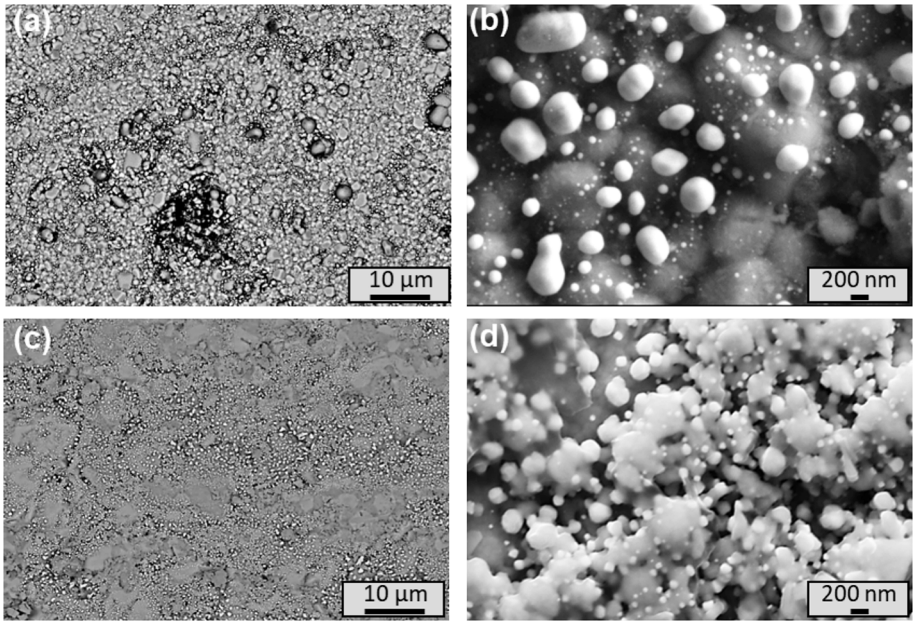

Fig. 8. SEM micrograph with backscattered (a,c) and SE (b,d) detector of the surface of a bare (a-b) and washcoated (c-d) membrane after permeation tests, highlighting the platinum distribution (bright particles).

Table 4
Activation energy of the tested membranes activated with Pt.

Membrane	T °C range	Ea (eV)
BCZY-GDC	T > 650	0.52
	T < 650	0.43
BCZY-GDC-WC	T > 650	0.29
	T < 650	0.33

specimen. Moreover, the BCZY-GDC-WC membrane shows similar activation energy values for hydrogen transport and water splitting reactions, indicating that the presence of a microporous layer on both sides of the membrane provides a symmetrical and effective dispersion of the catalytic platinum particles, increasing its active surface area, resulting in the acceleration of both processes. As a result, this leads to a reduced activation energy for the process, indicating that it occurs more readily compared to the bare membrane.

4. Conclusions

In this work, BCZY-GDC symmetric membranes with nanostructured coating of the same composite were manufactured and investigated for the first time. Stable water-based BCZY-GDC suspensions with Newtonian behavior and suitable viscosity of 0.01 Pa s were firstly obtained by the optimization of the amount of dispersant and the accurate rheological study of the slurries behavior containing different powder contents. The optimized 5 and 10 wt% BCZY-GDC suspensions were successfully used to produce nanostructured coating on symmetric BCZY-GDC membranes by dip coating. It was found that the quantity of material deposited increases with withdrawal speed, and the use of a centrifugation step to remove the excess solution after dip coating is of

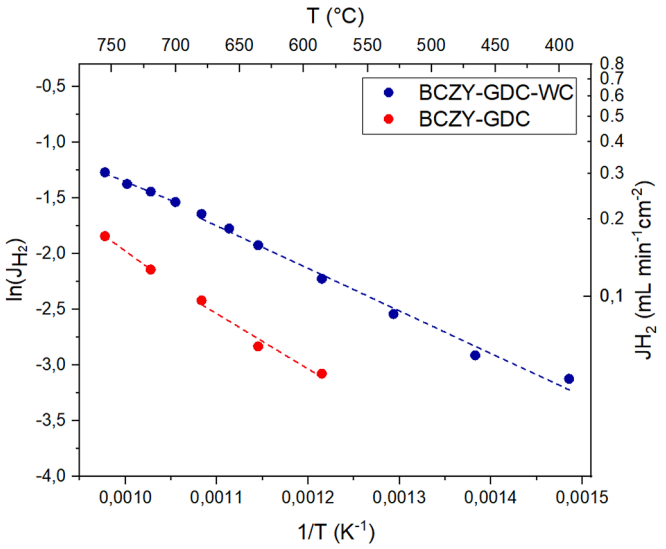

Fig. 9. Arrhenius plots of hydrogen fluxes for the bare (BCZY-GDC) and washcoated (BCZY-GDC-WC) membranes activated with Pt, feeding 50 % H2 in He with both humidified currents.

pivotal importance to avoid the formation of defects. Best results were obtained at v = 7 mm s^{-1} by using suspensions with the 10 wt% of solid loading. After 3 dips, the surface of symmetric membranes was homogeneously covered by a nanostructured, ≈3.5 μm thick porous coating.

The application of a nanostructured BCZY-GDC porous layer has been shown to enhance the membrane's specific surface area, significantly improving H_2 flux permeability – even in the absence of a catalyst – compared to the platinum-activated bare membrane. Moreover, washcoated membranes display enhanced hydrogen permeation compared to bare membranes activated with the same amount of catalyst due to the better dispersion of the Pt particles on the porous coating. At 750 °C, BCZY-GDC-WC membranes achieve permeation rates of 0.28 and 0.62 mL min^{-1} cm^{-2} using humidified feed streams with 50 and 80 % H_2 in He, respectively, which are among the highest reported in the literature for symmetric ceramic hydrogen separation devices. The deposition of a nanostructured washcoating, i.e. microporous layers on both sides of the membrane, using different types of catalytic materials opens the possibility of performing different reactions for hydrogen production, separation, and utilization, boosting the performance of the membrane reactor technology.

Declaration of competing interest

The authors declare that they have no known competing financial interests or personal relationships that could have appeared to influence the work reported in this paper.

Acknowledgments

This work has been funded by the agreement between Italian Ministry for the Environment and Energy Security and the Italian National Research Council "Ricerca di Sistema Elettrico Nazionale'', in the frame of the project "Frontier materials for energy applications".

Alessandra Sanson acknowledges Project code PE0000021, Concession Decree No. 1561 of 11.10.2022 adopted by Ministero dell'Università e della Ricerca (MUR), CUP B53C22004060006, Project title "Network 4 Energy Sustainable Transition—NEST", funded by the National Recovery and Resilience Plan (NRRP), Mission 4 Component 2 Investment 1.3—Call for tender No. 1561 of 11.10.2022 of Ministero dell'Università e della Ricerca (MUR), funded by the European Union—NextGenerationEU.

Jacopo De Maron acknowledges the National Recovery and Resilience Plan (NRRP), Mission 4 Component 2 Investment 1.3 - Call for tender No. 1561 of 11. 10. 2022 of Ministero dell'Università e della Ricerca (MUR); funded by the European Union – NextGenerationEU, PE0000021, "Network 4 Energy Sustainable Transition – NEST".

The publication has been realized by a researcher (Andrea Fasolini) with a research contract co-financed by the European Union - PON Ricerca e Innovazione 2014–2020, art. 24, comma 3, lett. a), della Legge 30 Dicembre 2010, n. 240 e s.m.i. e del D.M. 10 Agosto 2021 n. 1062.

The authors would like to thank Mr Cesare Melandri, Dr. Simone Casadio, and Mrs Guia Guarini for the optical microscope characterization, XRD analysis, and the contact angle measurements respectively.

Appendix A. Supplementary data

Supplementary data to this article can be found online at https://doi.org/10.1016/j.seppur.2025.133436.

References

[1] S. Van Renssen, The hydrogen solution? *Nat. Clim. Chang.* 10 (2020) 799–801, https://doi.org/10.1038/s41558-020-0891-0.
[2] O. Ališauskas. World Energy Outlook 2024.
[3] Roadmap for Sustainable Mixed Ionic-Electronic Conducting Membranes - Chen - 2022 - Advanced Functional Materials - Wiley Online Library Available online: https://onlinelibrary.wiley.com/doi/full/10.1002/adfm.202105702 (accessed on 13 June 2023).
[4] Global hydrogen development - A technological and geopolitical overview. *Int. J. Hydrogen Energy* 47 2022 7016–7048, doi:10.1016/j.ijhydene.2021.12.076.
[5] I. Stenina, A. Yaroslavtsev, Modern technologies of hydrogen production, *Processes* 11 (2022) 56, https://doi.org/10.3390/pr11010056.
[6] M.W. Melaina, O. Antonia, M. Penev, Blending hydrogen into natural gas pipeline networks: a review of key issues, *Renew. Energy* (2013).
[7] M. Nordio, S.A. Wassie, M. Van Sint Annaland, D.A. Pacheco Tanaka, J.L. Viviente Sole, F. Gallucci, Techno-economic evaluation on a hybrid technology for low hydrogen concentration separation and purification from natural gas grid, *Int. J. Hydrogen Energy* 46 (2021) 23417–23435, https://doi.org/10.1016/j.ijhydene.2020.05.009.
[8] J. Garcia-Fayos, J.M. Serra, M.W.J. Luiten-Olieman, W.A. Meulenberg. 8 - Gas Separation Ceramic Membranes. In *Advanced Ceramics for Energy Conversion and Storage*; Guillon, O., Ed.; Elsevier Series on Advanced Ceramic Materials; Elsevier, 2020; pp. 321–385 ISBN 978-0-08-102726-4.
[9] J.M. Serra, Electrifying chemistry with protonic cells, *Nat. Energy* 4 (2019) 178–179, https://doi.org/10.1038/s41560-019-0353-y.
[10] E. Mercadelli, A. Gondolini, M. Ardit, G. Cruciani, C. Melandri, S. Escolástico, J. M. Serra, A. Sanson, Chemical and mechanical stability of BCZY-GDC membranes for hydrogen separation, *Sep. Purif. Technol.* 289 (2022) 120795, https://doi.org/10.1016/j.seppur.2022.120795.
[11] C. Mortalò, E. Rebollo, S. Escolástico, S. Deambrosis, K. Haas-Santo, M. Rancan, R. Dittmeyer, L. Armelao, M. Fabrizio, Enhanced sulfur tolerance of $BaCe_{0.65}Zr_{0.20}Y_{0.15}O_{3-\delta}$-$Ce_{0.85}Gd_{0.15}O_{2-\delta}$ composite for hydrogen separation membranes, *J. Membr. Sci.* 564 (2018) 123–132, https://doi.org/10.1016/j.memsci.2018.07.015.
[12] W. Zhou, J. Malzbender, F. Zeng, W. Deibert, L. Winnubst, A. Nijmeijer, O. Guillon, R. Schwaiger, W.A. Meulenberg, Mechanical properties of $BaCe_{0.65}Zr_{0.2}Y_{0.15}O_3$ – $Ce_{0.85}Gd_{0.15}O_2$- dual-phase proton-conducting material with emphasis on micro-pillar splitting, *J. Eur. Ceram. Soc.* 42 (2022) 3948–3956, https://doi.org/10.1016/j.jeurceramsoc.2022.03.020.
[13] C. Mortalò, A. Santoru, C. Pistidda, E. Rebollo, M. Boaro, C. Leonelli, M. Fabrizio, Structural evolution of $BaCe_{0.65}Zr_{0.20}Y_{0.15}O_{3-\delta}$-$Ce_{0.85}Gd_{0.15}O_{2-\delta}$ composite MPEC membrane by in-situ synchrotron XRD analyses, *Mater. Today Energy* 13 (2019) 331–341, https://doi.org/10.1016/j.mtener.2019.06.004.
[14] E. Rebollo, C. Mortalò, S. Escolástico, S. Boldrini, S. Barison, J.M. Serra, M. Fabrizio, Exceptional hydrogen permeation of all-ceramic composite robust membranes based on $BaCe_{0.65}Zr_{0.20}Y_{0.15}O_{3-\delta}$ and Y- or Gd-doped ceria, *Energy Environ. Sci.* 8 (2015) 3675–3686, https://doi.org/10.1039/C5EE01793A.
[15] D. Montaleone, E. Mercadelli, S. Escolástico, A. Gondolini, J.M. Serra, A. Sanson, All-ceramic asymmetric membranes with superior hydrogen permeation, *J. Mater. Chem. A* 6 (2018) 15718–15727, https://doi.org/10.1039/C8TA04764B.
[16] V.M. Ievlev, G.S. Burkhanov, N.R. Roshan, E.K. Belonogov, A.A. Maksimenko, A. I. Dontsov, K.E. Rudakov, Structure, mechanical properties, and hydrogen permeability of Pd-Cu and Pd-Ru membrane foils prepared by magnetron sputtering, *Russ. Metall.* 2012 (2012) 994–1001, https://doi.org/10.1134/S0036029512110080.
[17] N.A. Al-Mufachi, N.V. Rees, R. Steinberger-Wilkens, Hydrogen selective membranes: a review of palladium-based dense metal membranes, *Renew. Sustain. Energy Rev.* 47 (2015) 540–551, https://doi.org/10.1016/j.rser.2015.03.026.
[18] M.A. Habib, A. Harale, S. Paglieri, F.S. Alrashed, A. Al-Sayoud, M.V. Rao, M. A. Nemitallah, S. Hossain, M. Hussien, A. Ali, et al., Palladium-alloy membrane

reactors for fuel reforming and hydrogen production: a review, *Energy Fuels* 35 (2021) 5558–5593, https://doi.org/10.1021/acs.energyfuels.0c04352.
[19] P. Gramazio, A. Bartoletti, A. Gondolini, E. Mercadelli, J. De Maron, E. Tosi Brandi, V. Saraceni, A. Fasolini, A. Sanson, F. Basile, High-temperature planar asymmetric ceramic membranes: effect of the Pt amount and dispersion on the H_2 separation performance, *J. Membr. Sci.* (2024) 123196, https://doi.org/10.1016/j.memsci.2024.123196.
[20] R.E. Hayes. *Introduction to Catalytic Combustion*; CRC Press LLC: Milton, 1998; ISBN 978-90-5699-092-3.
[21] W.B. Retallick, W. Chester. (54 WASHCOAT FOR A CATALYST SUPPORT.
[22] V. Palma, C. Ruocco, M. Cortese, M. Martino, Recent advances in structured catalysts preparation and use in water-gas shift reaction, *Catalysts* 9 (2019) 991, https://doi.org/10.3390/catal9120991.
[23] B. Mitra, D. Kunzru, Washcoating of different zeolites on cordierite monoliths: washcoating of different zeolites on cordierite monoliths, *J. Am. Ceram. Soc.* 91 (2007) 64–70, https://doi.org/10.1111/j.1551-2916.2007.02032.x.
[24] M.P. Lobera, S. Escolástico, J. Garcia-Fayos, J.M. Serra, Ethylene production by ODHE in catalytically modified $Ba_{0.5}Sr_{0.5}Co_{0.8}Fe_{0.2}O_3$− membrane reactors, *ChemSusChem* 5 (2012) 1587–1596, https://doi.org/10.1002/cssc.201100747.
[25] X. Tan, Z. Wang, H. Liu, S. Liu, Enhancement of oxygen permeation through $La_{0.6}Sr_{0.4}Co_{0.2}Fe_{0.8}O_{3-\delta}$ hollow fibre membranes by surface modifications, *J. Membr. Sci.* 324 (2008) 128–135, https://doi.org/10.1016/j.memsci.2008.07.008.
[26] S. Escolástico, C. Kjølseth, J.M. Serra, Catalytic activation of ceramic H_2 membranes for CMR processes, *J. Membr. Sci.* 517 (2016) 57–63, https://doi.org/10.1016/j.memsci.2016.06.017.
[27] B. Beyribey, J. Bayne, J. Persky, The effect of dip-coating parameters on the thickness and uniformity of BCZYZ electrolyte layer on porous NiO-BCZYZ Tubular supports, *Ceram. Int.* 48 (2022) 6046–6051, https://doi.org/10.1016/j.ceramint.2021.11.141.
[28] M. Faustini, B. Louis, P.A. Albouy, M. Kuemmel, D. Grosso, Preparation of sol−gel films by dip-coating in extreme conditions, *J. Phys. Chem. C* 114 (2010) 7637–7645, https://doi.org/10.1021/jp9114755.
[29] D. Montaleone, E. Mercadelli, A. Gondolini, M. Ardit, P. Pinasco, A. Sanson, Role of the sintering atmosphere in the densification and phase composition of asymmetric BCZY-GDC composite membrane, *J. Eur. Ceram. Soc.* 39 (2019) 21–29, https://doi.org/10.1016/j.jeurceramsoc.2018.01.043.
[30] A. Gondolini, A. Fasolini, E. Mercadelli, F. Basile, A. Sanson, Freeze cast porous membrane catalyst for hydrogen production via oxy-reforming, *Fuel Process. Technol.* 213 (2021) 106658, https://doi.org/10.1016/j.fuproc.2020.106658.
[31] S. Escolástico, C. Solís, C. Kjølseth, J.M. Serra, Outstanding hydrogen permeation through CO_2-stable dual-phase ceramic membranes, *Energy Environ. Sci.* 7 (2014) 3736–3746, https://doi.org/10.1039/C4EE02066A.
[32] A. Gondolini, A. Bartoletti, E. Mercadelli, P. Gramazio, A. Fasolini, F. Basile, A. Sanson, Development and hydrogen permeation of freeze-cast ceramic membrane, *J. Membr. Sci.* 684 (2023) 121865, https://doi.org/10.1016/j.memsci.2023.121865.
[33] A. Bartoletti, A. Sangiorgi, E. Mercadelli, C. Melandri, A. Gondolini, S. García-González, L. Ortiz-Membrado, M. Morales, E. Jimenez-Pique, A. Sanson, 3D microextrusion of eco-friendly water based cer-cer composite pastes for hydrogen separation, *Open Ceram.* 16 (2023) 100504, https://doi.org/10.1016/j.oceram.2023.100504.
[34] A. Gondolini, E. Mercadelli, S. Casadio, A. Sanson, Freeze cast support for hydrogen separation membrane, *J. Eur. Ceram. Soc.* 42 (2022) 1053–1060, https://doi.org/10.1016/j.jeurceramsoc.2021.10.063.
[35] V. Carnicer, C. Alcázar, M.J. Orts, E. Sánchez, R. Moreno, Microfluidic rheology: a new approach to measure viscosity of ceramic suspensions at extremely high shear rates, *Open Ceram.* 5 (2021) 100052, https://doi.org/10.1016/j.oceram.2020.100052.
[36] I.M. Krieger, Bingham award lecture—1989: the role of instrument inertia in controlled-stress rheometers, *J. Rheol.* 34 (1990) 471–483, https://doi.org/10.1122/1.550138.
[37] C. Baravian, D. Quemada, Correction of Instrumental inertia effects in controlled stress rheometry, *Eur. Phys. J. AP* 2 (1998) 189–195, https://doi.org/10.1051/epjap:1998183.
[38] T.E.R. Jones, J.M. Davies, A. Thomas, Fluid inertia effects on a controlled stress rheometer in its oscillatory mode, *Rheol. Acta* 26 (1987) 14–19, https://doi.org/10.1007/BF01332679.
[39] L.C. Almeida, F.J. Echave, O. Sanz, M.A. Centeno, J.A. Odriozola, M. Montes. Washcoating of Metallic Monoliths and Microchannel Reactors. In *Studies in Surface Science and Catalysis*; Gaigneaux, E.M., Devillers, M., Hermans, S., Jacobs, P.A., Martens, J.A., Ruiz, P., Eds.; Scientific Bases for the Preparation of Heterogeneous Catalysts; Elsevier, 2010; Vol. 175, pp. 25–33.
[40] L.D. Landau, B. Levich, Dragging of a liquid by a moving plate, *Acta Physicochim. URSS* 17 (1942), https://doi.org/10.1016/b978-0-08-010586-4.50053-5.
[41] W.A. Rosensteel, S. Ricote, N.P. Sullivan, Hydrogen permeation through dense $BaCe_{0.8}Y_{0.2}O_{3-\delta}$ – $Ce_{0.8}Y_{0.2}O_{2-\delta}$ composite-ceramic hydrogen separation membranes, *Int. J. Hydrogen Energy* 41 (2016) 2598–2606, https://doi.org/10.1016/j.ijhydene.2015.11.053.
[42] Y. Yang, Y. Zeng, B.S. Amirkhiz, J.-L. Luo, N. Yan, Promoting the ambient-condition stability of Zr-doped barium cerate: toward robust solid oxide fuel cells and hydrogen separation in syngas, *J. Power Sources* 378 (2018) 134–138, https://doi.org/10.1016/j.jpowsour.2017.12.036.
[43] S. Escolastico, J. Seeger, S. Roitsch, M. Ivanova, W.A. Meulenberg, J.M. Serra, Enhanced H_2 separation through mixed proton–electron conducting membranes based on $La_{5.5}W_{0.8}M_{0.2}O_{11.25}$, *ChemSusChem* 6 (2013) 1523–1532, https://doi.org/10.1002/cssc.201300091.
[44] M.E. Ivanova, S. Escolástico, M. Balaguer, J. Palisaitis, Y.J. Sohn, W. A. Meulenberg, O. Guillon, J. Mayer, J.M. Serra, Hydrogen separation through tailored dual phase membranes with nominal composition $BaCe_{0.8}Eu_{0.2}O_{3-\delta}$: $Ce_{0.8}Y_{0.2}O_{2-\delta}$ at intermediate temperatures, *Sci. Rep.* 6 (2016) 34773, https://doi.org/10.1038/srep34773.